

Understanding Pressure Vessel Steels: An Atom Probe Perspective

M. K. Miller,* P. Pareige,*[†] and M. G. Burke[‡]

**Microscopy and Microanalytical Sciences Group, Metals and Ceramics Division, Oak Ridge National Laboratory, Oak Ridge, TN 37831-6376; [†]Groupe de Metallurgie Physique, UMR CNRS 6634, Faculté des sciences de l'université de Rouen, 76128 Mont Saint Aignan, France; and [‡]Bechtel Bettis, Inc., West Mifflin, PA 15122*

A review of the contributions of the atom probe field-ion microscopy (APFIM) technique to the microstructural characterization of pressure vessel steels and to the understanding of the embrittlement of these materials during neutron irradiation is presented. Atom probe studies have revealed that the microstructure contains a variety of ultrafine clusters and precipitates some of which are only formed during neutron irradiation. Furthermore, there is a complex pattern of segregation of various solutes (including phosphorus, nickel, manganese, or molybdenum) to grain boundaries in some pressure vessel materials, and there may also be additional intergranular precipitation in these materials. Published by Elsevier Science Inc.

INTRODUCTION

Since the introduction of the atom probe field-ion microscope (APFIM) [1, 2] in 1967, it has been used extensively for the characterization of steels that are used in the pressure vessels of nuclear reactors. The primary aim of these studies has been to characterize the microstructural features that are responsible for the embrittlement of these materials that occurs during service, and to evaluate postirradiation annealing treatments designed to restore the mechanical properties. The embrittlement of these materials is clearly evident from the mechanical properties in an increase in the ductile-to-brittle transition temperature, a reduction in fracture toughness, and a loss in the upper shelf energy [3–8]. The embrittlement has been correlated with the levels of copper, phosphorus, nickel, and manganese in the steel. In particular, the steel welds in some of the first commercial reactors are a special concern because of the elevated copper content of the welds, which was primarily due to the use of cop-

per-coated welding rods in the welding process. Because the service temperature of these materials is relatively low, typically 288°C, the thermal diffusion of solute is extremely slow. Although radiation-enhanced diffusion may significantly increase solute transport, the scale of the microstructural features that develop is likely to be extremely small, and are generally under the resolution of conventional techniques.

The atom probe is a particularly powerful tool for the characterization of these materials due to its high spatial resolution, light element sensitivity, and ability to quantify the composition of ultrafine (<5nm) precipitates [2, 9]. The atom probe technique has provided valuable information about ultrafine precipitates, solute clustering, and segregation to lath and grain boundaries. The size, shape, and number density of these ultrafine features are obtained from high magnification images in the field ion microscope. The composition of these features and the matrix have been obtained from both the classic atom probe (i.e., the straight time-of-flight

atom probe and the energy-compensated instrument) and from atomic level reconstruction of the positions of solute atoms obtained in the three-dimensional atom probe (3DAP). The relatively low doses of neutron radiation and the extremely small volume and activity of a typical field ion specimen of these materials do not impose significant difficulties in the preparation of specimens if appropriate safety precautions are followed [9].

Several other techniques have been used in attempts to characterize the microstructures of these materials with varying degrees of success. The main alternatives to atom probe field ion microscopy are small angle neutron scattering (SANS) and transmission electron microscopy. However, both of these techniques suffer from serious limitations in the characterization of these ferromagnetic materials. Although the SANS technique is able to gather information from a large volume of material, the interpretation of that data requires a valid model, and the data are subject to multiple interpretations as to the solute and vacancy contents of the features present. In addition, SANS cannot reliably deconvolute the contributions from the multiple types of precipitates present in these materials or distinguish between intergranular or intragranular precipitates. However, the results obtained in the atom probe may be used to provide a reliable framework for the interpretation of SANS data. Transmission electron microscopy of these types of steels is extremely sensitive to specimen preparation artifacts, such as the redeposition of copper on the surface of the thin-foil specimen and surface oxidation. Furthermore, these irradiation-induced clusters do not generate sufficient contrast for imaging in the transmission electron microscope. In addition, quantification of the composition of small features (<5nm) in the analytical transmission electron microscope is extremely difficult or impossible due to their size, the presence of significant composition gradients around the features, and the interaction volume of the electron beam and the thickness of the specimens.

In this paper, a review of the contributions of the atom probe technique to the understanding of the embrittlement of pressure vessel steels is presented. Atom probe studies have been performed on plate, forged components and welds from surveillance materials, materials obtained from decommissioned reactors, and test reactor-irradiated materials [9–32]. In addition, unirradiated control material, long-term thermally aged materials, and model alloys have also been examined [33–43]. These characterizations have revealed that the microstructure of the matrix of commercial pressure vessel steels is extremely complex and involves many different types of intragranular features including copper and phosphorus clusters and precipitates, carbides, nitrides, and oxides. In addition, atom probe studies have revealed a complex pattern of segregation of various solutes including phosphorus, nickel, manganese, molybdenum, and nitrogen to grain boundaries, and have also documented the extent of intergranular precipitation. These phenomena are a potential source of embrittlement because solute segregation and intragranular and intergranular precipitation can significantly alter the mechanical properties of the matrix and grain boundaries and even promote mechanisms such as temper embrittlement. In addition, the hardening of the matrix from the formation of intragranular clusters and precipitates will make the mechanical properties of the grain boundaries more important because the steel will generally fail at the weakest link.

MICROSTRUCTURE AFTER NEUTRON IRRADIATION

Most of the early atom probe studies focussed on Western pressure vessel steels. These steels have included an A302B plate and several A533B type steels and welds. Some typical compositions of these steels are given in Table 1. In addition to these steels, a ferritic–bainitic 16MND5-type steel from the French surveillance program and

a vanadium-containing plate steel from the Gundremmingen KRB-A reactor have been examined. Recently, atom probe characterizations have been performed on the significantly different 15Kh2MFA Cr–Mo–V and 15Kh2NMFA Ni–Cr–Mo–V pressure vessel steels used in Russian VVER 440 and VVER 1000-type nuclear reactors, respectively.

SETTING THE STAGE

The first atom probe study of neutron-irradiated pressure vessel steels was performed by Miller and Brenner in 1981 on an A302B plate steel from a surveillance capsule [10, 11]. This steel had a composition (atom percent—at. %) of Fe-0.17% Cu-0.17% Ni-1.35% Mn-0.45% Si-0.29% Mo-0.12% Cr-0.08% Al-1.1%, C-0.02% P-0.03% N-0.04% S, and was irradiated for 8 years at 290°C to a fluence of $2.2 \times 10^{23} \text{ n m}^{-2}$. After this exposure, the copper and phosphorus levels in the matrix were found to be significantly reduced to 0.01 at. % Cu and 0.005 at. % P, respectively. However, it was established later that some preferential evaporation of copper had occurred during the analysis, and so these figures are probably a slight underestimate of the actual levels in the matrix. A high density of ultrafine ($< \sim 10 \text{ nm}$) darkly imaging copper-enriched features was observed in the matrix of the neutron-irradiated steel, as shown in Fig. 1. These copper-enriched regions were enriched in other solutes including phosphorus and aluminum. In addition to the copper-enriched regions, some ultrafine phospho-

rus-enriched regions and some 1nm-diameter spherical and needle-shaped Mo_2C precipitates were also observed, as shown in Fig. 2. Large Mo_2C precipitates were also analyzed in the unirradiated and irradiated materials. The composition of one of these precipitates was reported as 56 at. % Mo-8% Fe-1% Cr-35% C. No solute segregation at the carbide matrix interface was observed. In contrast, segregation was observed at both cementite–ferrite interfaces and at grain boundaries in this A302B steel, as shown in Fig. 3 by the brightly imaging decoration. Atom probe analysis revealed that Mo, C, V, Cr, and Co were enriched at the cementite–ferrite interface and the grain boundaries.

These and some additional features have subsequently been observed in many other neutron-irradiated pressure vessel steels and can be divided into four general categories: matrix composition, ultrafine ($< \sim 10 \text{ nm}$) precipitates, coarse ($> \sim 10 \text{ nm}$) precipitates, and segregation to boundaries. These categories will be discussed in detail in the following sections.

MATRIX

The characterization of the composition of the matrix is important, as the solute concentrations are required to provide a mass balance and also to establish the baseline for the determination of the solute enrichment factors. The composition of the matrix is also required to establish the concentrations of the alloying elements as a function of different steps in the heat treatment. It is

Table 1 Typical Nominal Compositions of Pressure Vessel Steels

Alloy	Cu	Ni	Mn	Si	Mo	Cr	V	Al	C	P	S
A302B	0.17	0.17	1.35	0.45	0.29	0.12	—	0.08	1.1	0.02	0.04
A533B	0.2–0.35	0.57	1.37	1.01	0.25	0.05	—	—	0.55	0.011	0.022
16MND5	0.078	0.53	1.26	0.63	0.22	0.17	0.021	0.05	0.74	0.021	0.009
KRB-A	0.14	0.71	0.71	0.43	0.36	0.41	0.04	0.08	1.01	0.023	0.021
15Kh2MFA	0.30	0.07	0.36	0.36	0.39	2.77	0.33	—	0.67	0.032	0.052
15Kh2NMFA	0.05	1.15	0.41	0.49	0.34	2.49	0.11	—	0.79	0.016	0.009

The balance is iron and these data are presented in atomic percent.

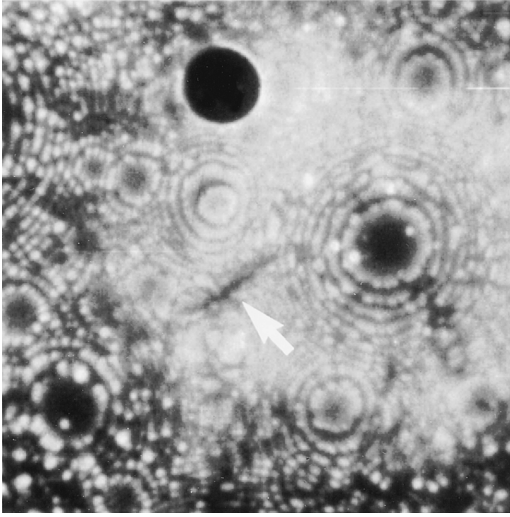


FIG. 1. Field ion micrograph of an ultrafine darkly imaging copper-enriched feature in the matrix of the neutron-irradiated A302B plate steel.

also important that contributions from ultrafine features are not included in the matrix composition so that these parameters can be determined accurately. Several statistical tools were developed specifically to assist in this process [2, 9].

Atom probe studies have revealed the importance of the stress-relief treatment in high copper ($> \sim 0.2 \text{ at.} \% \text{ Cu}$) weld materials. It has been established that the copper level that remains in the matrix in high copper alloys after the stress-relief treatment and before neutron irradiation is strongly dependent on the annealing temperature and the cooling rate to room temperature. The measured copper levels have been

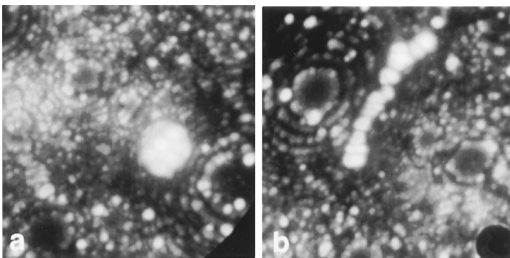


FIG. 2. Field ion micrograph of 1nm-diameter spherical and needle-shaped Mo_2C precipitates in the matrix of the neutron-irradiated A302B plate steel.

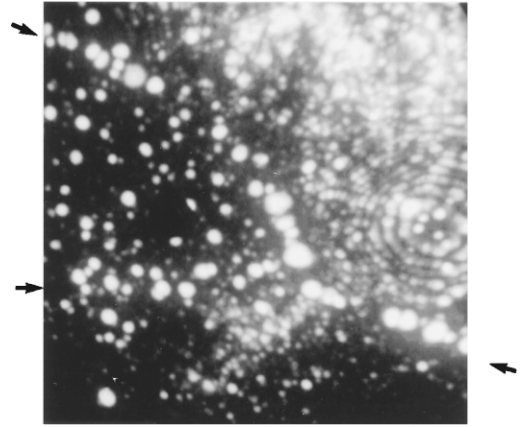


FIG. 3. Field ion micrograph of a cementite precipitate at a grain boundary in a neutron-irradiated A302B steel plate. Both cementite–ferrite interfaces and ferrite–ferrite interfaces are decorated by a thin film of molybdenum carbonitride precipitates.

found to be in good agreement with thermodynamic predictions. These studies have concluded that a lower annealing temperature and a longer time is most effective in minimizing the susceptibility of these materials to embrittlement due to copper [19].

The copper level in the matrix after neutron irradiation has been measured in several pressure vessel steels, and the results are summarized in Table 2. It is evident from these results that a significant depletion in the copper content occurs after neutron irradiation. There is a general trend at low fluences that the copper level decreases with increasing fluence. The minimum level of copper in the matrix is approximately 0.04 to 0.05 at. % Cu. No significant difference has been found between the different types of steels. The copper levels measured do not agree well with extrapolation of high-temperature thermal annealing data or equilibrium thermodynamic predictions in model iron–copper alloys. This discrepancy is not surprising, because the neutron irradiation increases the number of point defects present in the matrix, and hence, changes the free energy of the system. This change will alter the position of the phase fields in the phase diagram. This

Table 2 Comparison of the Copper Contents in the Matrix of a Variety of Neutron-Irradiated Pressure-Vessel Steels

Reference	Steel	Fluence $n\ m^{-2}$	Nominal at. % Cu	Matrix at. % Cu
[17, 18]	A533-B	2×10^{21}	0.13	0.10 ± 0.03
[17, 18]	KRB-A	8.4×10^{21}	0.14	0.13
[17, 18]	KRB-A	2×10^{22}	0.14	0.12
[17, 18]	KRB-A	2.7×10^{22}	0.14	0.11 ± 0.01
[23]	Chooz	4.7×10^{22}	0.08	0.05 ± 0.01
[34]	Weld	6.6×10^{22}	0.14	0.13 ± 0.04
[17, 18]	KRB-A	8.5×10^{22}	0.14	0.09 ± 0.01
[33]	Weld	1.1×10^{23}	0.18 to 0.28	0.06 ± 0.01
[13, 14]	Rolls Royce	2×10^{23}	0.2	0.1
	Weld	2.0×10^{23}	0.27	0.06 ± 0.01
[23]	Chooz	2.5×10^{23}	0.08	0.04 ± 0.01
[34]	Weld	3.5×10^{23}	0.14	0.05 ± 0.01
[23]	Chooz	6.6×10^{23}	0.08	0.03 ± 0.04
[23]	Chooz	1.2×10^{24}	0.08	0.04 ± 0.01

effect has been observed in neutron-irradiated Fe–Cr alloys [44].

Composition variations of the other elements in the alloy, particularly nickel, manganese, phosphorus, and silicon, are present, but are not as distinct as those of copper. In addition, the matrix composition of the steels is always different from the alloy composition due to the formation of coarse precipitates that depletes the matrix of the elements that are consumed in these precipitates (typically carbon, molybdenum, chromium, and vanadium). This effect varies with the different types of steels.

ULTRAFINE CLUSTERS AND PRECIPITATES

The most common characteristic of the neutron-irradiated pressure vessel steels is the presence of darkly imaging copper-enriched features, which are not observed in unirradiated materials. Two different morphologies have been observed. Most of these features were found to be roughly spherical, but a few examples of elongated ribbons have also been observed. It has been speculated that the ribbon morphology is a result of copper segregation to a moving dislocation. The size of these spherical features was found to be between ~ 1 and 4 nm. Sev-

eral other solutes have been detected in the copper-enriched features. It has already been mentioned that phosphorus and aluminum were observed in A302B steel. Phosphorus has also been detected in a large proportion of these features in other steels.

The microstructural development in neutron-irradiated weldments was evaluated for materials from H. B. Robinson II and from a Rolls Royce test program by Burke and Brenner using APFIM [13, 14]. In addition to the identification of copper-enriched solute clusters in the irradiated microstructure, Burke and Brenner also provided the first evidence of Mn and Ni enrichments associated with these irradiation-induced clusters. These irradiation-induced features were termed “solute-rich clusters” because they contained significant amounts of copper, manganese, nickel, silicon, and occasionally phosphorus, as well as high levels of iron. The H. B. Robinson II data also included examples that suggested that the irradiation-induced clusters had a copper-enriched core with manganese and nickel surrounding the core. Burke and Brenner observed that manganese and nickel were also enriched in these features in a high nickel and high manganese neutron-irradi-

ated weld from a Rolls Royce test program (Fe-0.2 at. % Cu-1.5% Ni-1.6% Mn-0.9% Si-0.2% Mo) [14]. Manganese, nickel, and silicon enrichments have also been observed in A533B and other steels. Atom probe composition profiles revealed that the spatial extent of the manganese, nickel, and silicon enrichments was generally slightly larger than that of the copper, as shown in Fig. 4. A set of atom maps of some of these features in a weld (Fe-0.27 at. % Cu-1.58% Mn-0.57% Ni-0.34% Mo-0.27% Cr-0.58% Si-0.003% V-0.45% C-0.009% P-0.009% S) after neutron irradiation to a fluence of $2 \times 10^{21} \text{ n m}^{-2}$ ($E > 1 \text{ MeV}$) is shown in Fig. 5. In the 16MND5 steel from the Chooz A reactor, Pareige et al. [30] found that the number density of 3 to 4 nm diameter copper-enriched clusters increased from 3.3×10^{23} to $11 \times 10^{23} \text{ m}^{-3}$ with increasing fluence 2.5 to $16 \times 10^{23} \text{ n m}^{-2}$ ($E > 1 \text{ MeV}$). These results were found to be in good agreement with SANS data. The composition of the clusters was found to be Fe \sim 1 at % Cu \sim 4% Ni \sim 5% Mn \sim 3% Si did not appear to change significantly with increasing fluence.

The copper levels measured in these features (\sim 1 to \sim 30% Cu) in neutron-irradiated materials are always substantially below the equilibrium copper level of the

ϵ copper precipitate. Copper invariably has the highest enrichment factor over the matrix level, although the absolute copper level measured may be less than the absolute levels of manganese and nickel in the clusters in some cases. This effect is due to the significantly lower initial level of copper in the matrix of the steel compared to either nickel or manganese after the stress-relief treatment. It was also evident that these features contained significant levels ($>70\%$) of iron.

These features have been referred to as copper-enriched clusters, zones, precipitates, and copper-stabilized microvoids. One of the main difficulties in establishing the true identity of these small features is the lack of proper definitions of what these terms mean at ultrahigh resolution. A cluster is simply an aggregate of solute atoms within the matrix with no distinct interface, whereas a precipitate is generally defined as a region of solute with a well-defined crystal structure and interface with the matrix. Copper is a substitutional atom in the body centered cubic (or body centered tetragonal) iron lattice, and copper precipitates (ϵ Cu) in iron are face-centered cubic (fcc). It is thought that the copper forms an intermediate body-centered cubic precipitate as a precursor to the fcc structure [45]. A high-resolution transmission electron microscopy analysis of precipitates in aged Fe-1.3at.% Cu and Fe-1.3at.% Cu-1.1% Ni alloys by Othen et al. [46] indicated that the structure of fine precipitates formed during thermal aging is 9R. Similar structures have not yet been observed in pressure vessel steels. The cluster vs. precipitate identification is further complicated when other solutes and composition gradients are involved. It should be noted that a diffuse solute-enriched cluster or well-defined precipitates containing larger numbers of copper atoms would both impede the motion of dislocations through the microstructure, and therefore, have an effect on the mechanical properties. Although vacancies have been imaged in the field ion microscope in pure elements and ordered compounds [2], it is not possible to establish the

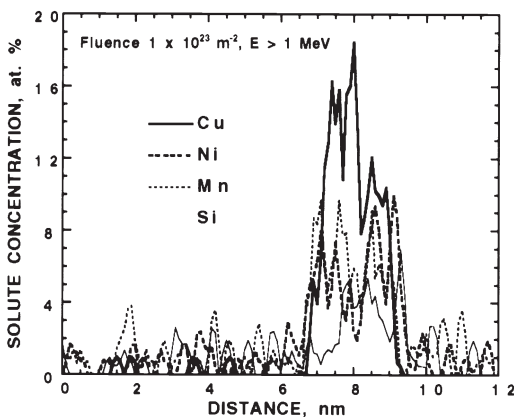


FIG. 4. Atom-probe composition profiles across a copper-enriched feature in a neutron-irradiated A533B submerged arc weld showing that the spatial extent of the manganese, nickel, and silicon enrichments was generally slightly larger than that of the copper.

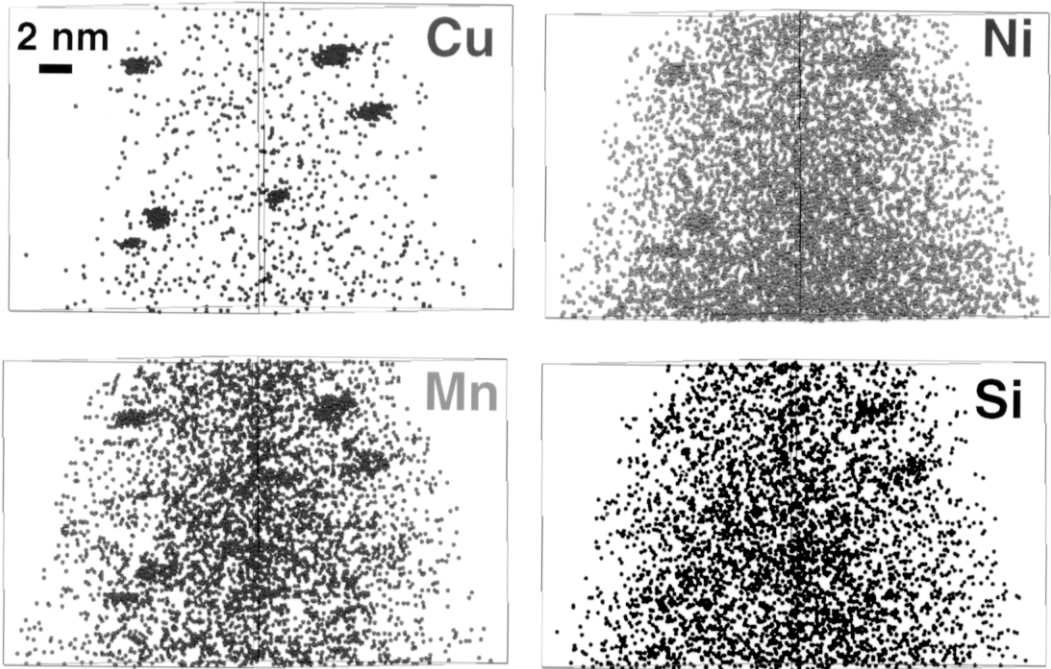


FIG. 5. Atom maps of the copper, manganese, nickel, and silicon distribution in a submerged arc weld neutron-irradiated to a fluence of $2 \times 10^{23} \text{ n m}^{-2}$ ($E > 1 \text{ MeV}$) obtained in a three-dimensional atom probe. Note the solute-enriched regions that result from neutron irradiation.

presence or concentration of vacancies in these features in these complex steels from either their appearance in the images in the field ion microscope or from compositional determinations in the atom probe.

Atom-probe analyses have also revealed the presence of phosphorus clusters. They can sometimes be distinguished from the darkly imaging copper features by the presence of some bright spots on the darkly imaging background, as shown in Fig. 6. These $\sim 1 \text{ nm}$ diameter clusters are generally observed only in high phosphorus steels or when the copper level is extremely low. These phosphorus clusters are often associated with nickel enrichments.

Another common microstructural feature is the ultrafine, brightly imaging spherical and needle-shaped molybdenum carbide and disc-shaped molybdenum nitride precipitates. Some of these precipitates were found to be only $\sim 1 \text{ nm}$ in diameter. These precipitates have been observed in A302B plate [11] and A533B plate and weld material [9, 15, 17, 18, 24] and in material from

the Gundremmingen KRB-A reactor [17, 24]. These precipitates have been observed in both unirradiated and neutron-irradiated materials. The distribution of these features in the steel was generally found to be relatively inhomogeneous. Their number density was typically slightly lower than that of

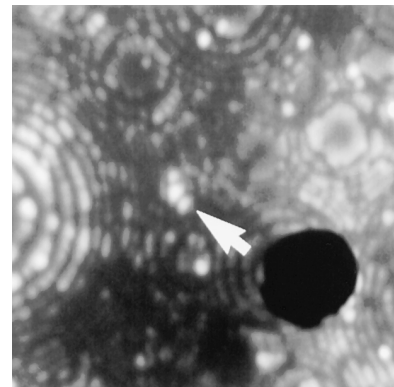


FIG. 6. Field ion micrograph of a phosphorus cluster in a neutron-irradiated VVER 440 pressure vessel steel.

the copper-enriched features. Insufficient data exist to conclusively establish whether there is a change in the number density of these features after neutron irradiation and whether these precipitates are responsible for some of the embrittlement observed during neutron irradiation. Isolated examples of small darkly imaging oxide precipitates have also been observed [19].

Pareige et al. [32] also detected decoration of molybdenum and phosphorus atoms at dislocations in an unirradiated forging, as shown by the bright spots decorating the dislocation in Fig. 7. No attempts have been made to study the possible segregation to dislocation or interstitial loops in the irradiated materials.

COARSE PRECIPITATES

Coarse precipitates are present in low number densities in the interior of the grains, at grain boundaries, and on dislocations. These coarse precipitates are present in both the unirradiated and neutron-irradiated materials. The compositions of these precipitates are important parameters in determining the location and levels of all the solutes in the steel. It should be noted that the size of these coarse precipitates are

normally larger than the field of view of the field ion microscope (typically $\sim 100\text{nm}$), so size measurements are generally estimated from the transmission electron microscope.

A 200 to 600nm fcc copper–manganese precipitate was observed on a grain boundary in a neutron-irradiated A533B submerged arc weld [15, 18], as shown in Fig. 8. The composition of the central portion of this coarse precipitate was determined to be 83.6 ± 1.2 at. % Cu, $14.5 \pm 1.1\%$ Mn, $1.5 \pm 0.4\%$ Ni, and $0.3 \pm 0.2\%$ Fe. The precipitate–matrix interface was also found to be substantially enriched in manganese and nickel, as shown in Fig. 9. These coarse copper–manganese precipitates are often formed at grain boundaries and dislocations during the initial treatment of the alloy or the stress-relief treatment and subsequent cooling. They account for the difference between the nominal copper content of the alloy and the measured matrix copper level after the stress relief treatment.

Coarse (~ 0.1 to $0.5\mu\text{m}$) darkly imaging cementite precipitates have been observed in A302B, as noted above, and in A533B and the Gundremmingen KRB-A and the Russian VVER 440 and 1000 steels. A summary of the compositions of these cementite precipitates is given in Table 3. The com-

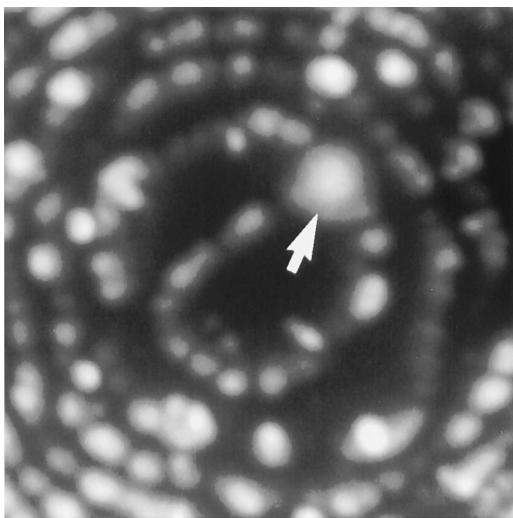


FIG. 7. Field ion micrograph of molybdenum and phosphorus atoms decorating a dislocation in an unirradiated forging.

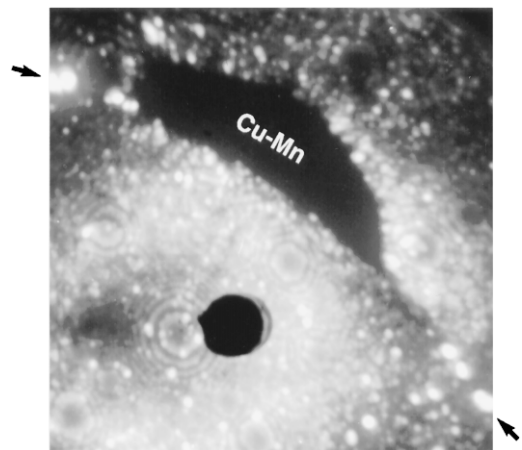


FIG. 8. Field ion micrograph of a darkly imaging copper–manganese precipitate at a grain boundary (arrowed) in a neutron-irradiated A533B submerged arc weld.

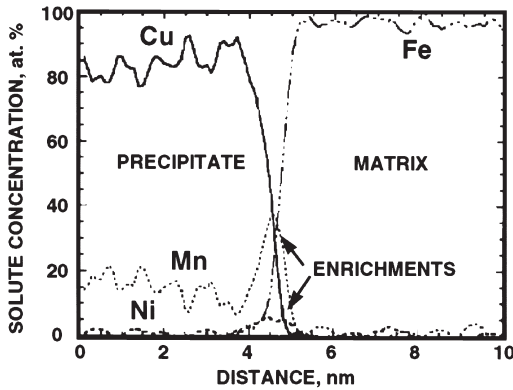


FIG. 9. Atom-probe composition profile from the center of the copper–manganese precipitates shown in Fig. 8 into the ferrite matrix. The interface was also found to be substantially enriched in manganese and nickel.

position of the cementite was found to depend on the composition of the steel. The enrichment of solutes in these precipitates accounts for some of the depletion of these elements in the matrix analyses.

Coarse brightly imaging Mo_2C precipitates have been observed in A533B submerged arc weld, as shown in Fig. 10(a). A summary of the compositions of these precipitates is given in Table 4. Phosphorus enrichment at the carbide–matrix interface has been observed. The enrichment of solutes in these precipitates accounts for some of the depletion of these elements in the matrix analyses.

Smaller brightly imaging roughly spherical $V(C,N)$ precipitates have been characterized in both vanadium-containing Gundremmingen KRB-A and the Russian VVER 440 and 1000 steels. A ~ 10 nm diameter $V(C,N)$ precipitate in the ferrite matrix of the Gundremmingen KRB-A reactor steel is shown in Fig. 10(b). This precipitate contained virtually no molybdenum, manganese, or chromium. Phosphorus was detected in the precipitate and in the ferrite matrix adjacent to the precipitate. Similar precipitates were observed in the matrix and at boundaries in the Russian VVER 440 and 1000 steels [25–29], as shown in Figs. 10(c) and (d). The average composition of these precipitates in a neutron-irradiated high-phosphorus weld (Fe-1.7 at. % Cr-0.37% Mo-0.2% V-0.95% Mn-0.14% Ni-0.69% Si-0.23% C-0.12% Cu-0.058% P) was determined to be 51.3 ± 0.9 at. % V- $18.8 \pm 0.7\%$ C- $22.1 \pm 0.7\%$ N- $4.9 \pm 0.4\%$ Cr- $2.3 \pm 0.3\%$ Mo- $0.36 \pm 0.05\%$ Fe- $0.07 \pm 0.05\%$ B- $0.03 \pm 0.03\%$ P.

Blocky M_7C_3 carbides have also been observed in the Russian VVER 440 and 1000 steels [26, 27]. An atom probe analysis of one of these darkly imaging precipitates in the VVER 440 steel yielded a composition of 37.6 ± 1.7 at. % Cr- $22.7 \pm 1.4\%$ Fe- $3.5 \pm 0.6\%$ Mo- $2.7 \pm 0.6\%$ V- $0.6 \pm 0.3\%$ Mn- $33.0 \pm 1.6\%$ C. No nitrogen, nickel, silicon, or copper was detected in this precipitate. Transmission electron microscopy of these pre-

Table 3 Composition of Cementite Precipitates as Measured by the Atom Probe in Different Pressure Vessel Steels

Solute [Ref.]	A302B 2.2×10^{23} $n m^{-2}$ [10, 11]	16MND5 1.4×10^{24} $n m^{-2}$ [20]	16MND5 >28 h at 600°C [20]	SA-533 Plate 29 h at 593–621°C [32]	SA-533 Plate 93,000 h at 280°C [32]
Fe	balance	60.0 ± 1.1	61.5 ± 0.7	64.0 ± 0.8	61.1 ± 0.1
Mn	9.3	9.4 ± 0.7	10.4 ± 0.5	8.7 ± 0.5	11.9 ± 0.7
Mo	2.6 to 16	1.65 ± 0.3	1.3 ± 0.2	1.2 ± 0.2	0.9 ± 0.2
Cr	1.3	2.6 ± 0.4	1.7 ± 0.2	0.5 ± 0.1	—
Ni	—	0.7 ± 0.2	0.7 ± 0.1	—	0.2 ± 0.1
Si	—	0.11 ± 0.07	0.07 ± 0.04	—	—
C	25 ^a	25.5 ± 1.0	22.3 ± 0.7	25.6 ± 0.7	25.4 ± 0.9

Data are in atomic percent.
^a Normalized to 25% C.

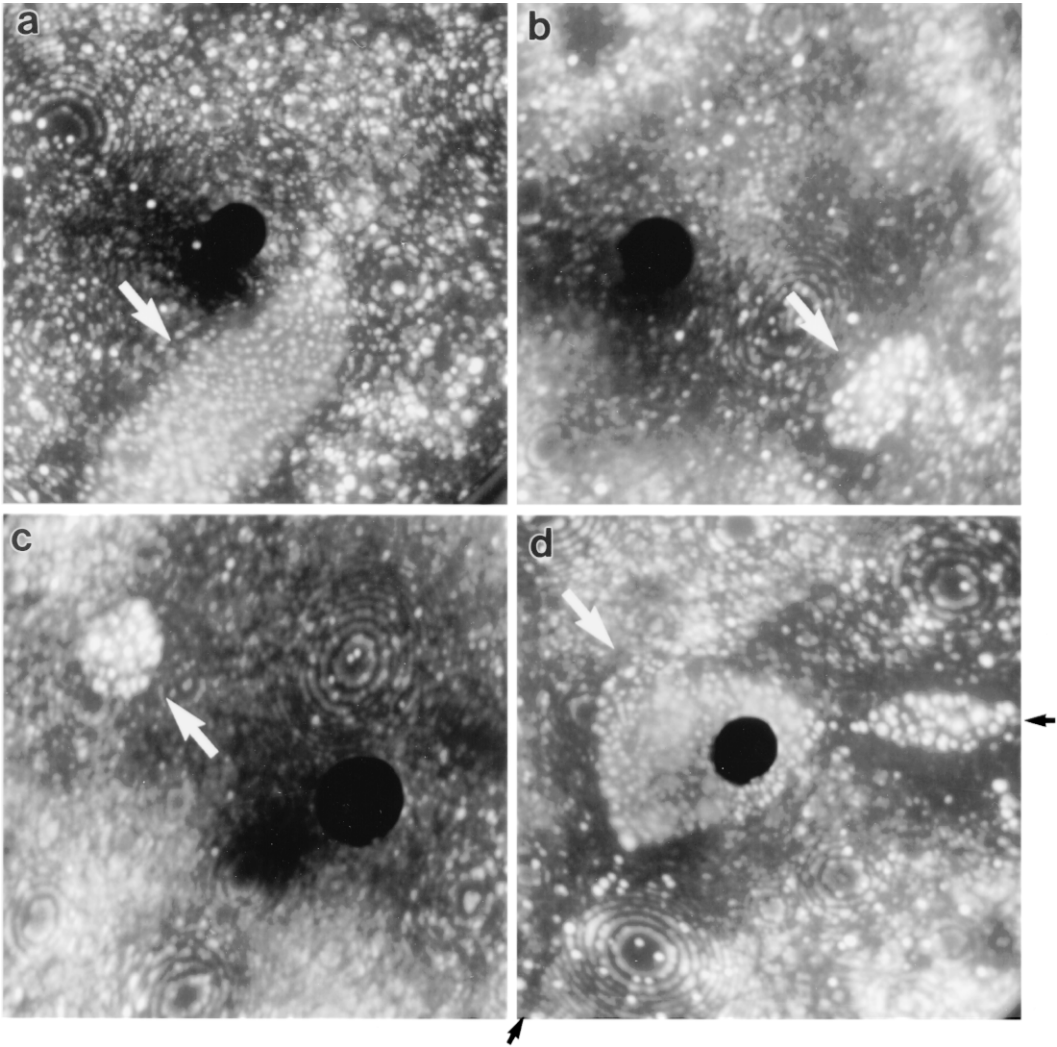


FIG. 10. Field ion micrographs of (a) a brightly imaging Mo_2C precipitate in a neutron-irradiated A533B submerged arc weld, (b) a $\sim 10\text{nm}$ diameter $\text{V}(\text{C},\text{N})$ precipitate in the ferrite matrix of the Gundremmingen KRB-A reactor steel, (c) $\text{V}(\text{C},\text{N})$ precipitates in the matrix, and (d) at a boundary in Russian VVER 440 and 1,000 steels.

precipitates revealed a characteristic faulted structure and a size range of 60 to 300nm and 60 to 500nm in the VVER 440 and 1000 steels, respectively.

SEGREGATION TO BOUNDARIES

Recently, the susceptibility of Russian pressure vessel steels to temper embrittlement has become a serious concern for continued safe operation. This concern is primarily due to the high phosphorus levels that

have been measured in the bulk materials and the observation of intergranular fracture in some materials. Although the maximum permissible levels for phosphorus and sulphur are 0.020 wt. % in the 15Kh2NMFA steel and 0.025 wt. % in the 15Kh2MFA steel, a number of cases have been found where these values were exceeded.

A general characteristic of the steels is that the grain and lath boundaries are decorated with solutes, and this is manifested as some brightly imaging spots in the field ion

micrographs, as shown in Fig. 3 for an A302B steel and Figs. 11(a) and (b) for an A533B and a Russian VVER 440 steel. Atom probe analysis has established that these brightly imaging spots are a thin semicontinuous film of molybdenum carbonitride precipitates. In addition, the boundaries generally exhibit phosphorus segregation.

The amount of solute segregation at interfaces may be estimated with the use of a method based on the Gibbsian interfacial excess [27, 47]. The Gibbsian interfacial excess of element i , Γ_i , may be determined directly from an atom probe analysis for all elements with the use of the following relationships:

$$\Gamma_i = N_{i(\text{excess})}/A = N_i - N_{i(\alpha)} - N_{i(\beta)}/A \quad (1)$$

where $N_{i(\text{excess})}$ is the excess number of solute atoms associated with the interface, N_i is the total number of solute atoms in the volume analyzed, $N_{i(\alpha)}$ and $N_{i(\beta)}$ are the number of solute atoms in the two adjoining regions α and β either side of the dividing surface, and A is the interfacial area over which the interfacial excess is determined. This method provides a fundamental estimate of the level of segregation at an interface.

The phosphorus coverage measured at some boundaries in both an A533B and Russian steels is summarized in Table 5 [27–29]. It is evident that the phosphorus

coverage at the boundary increases with neutron irradiation and with the initial phosphorus level in the steel. With the exception of the neutron-irradiated Weld 37 material, the fracture surface of all these materials was found to be transgranular. It has been suggested that because the level of phosphorus at the boundaries is significantly higher than that required to produce intergranular failure in binary Fe–P alloys, the carbon or the carbonitride film at the boundaries is playing an important role in suppressing a change in failure mode.

Because the parameters for phosphorus segregation are reasonably well established in steel [48, 49], the atom-probe results from the unirradiated materials have been compared with predictions from the McLean model of equilibrium segregation [50]. A free energy change of $\Delta G_p = -56,700 + 12.4 T$ was used in these calculations [49]. A comparison of the measured and predicted values for some boundaries in unirradiated pressure vessel steels is shown in Table 5 [27–29]. Excellent agreement between the measured and predicted values was found. It was also noted that these model predictions indicate that the phosphorus coverage at the boundary will increase significantly with postirradiation annealing, and so it was recommended that this method should be avoided in high phosphorus steels.

Table 4 Composition of Some Typical Coarse Mo₂C Precipitates as Measured by the Atom Probe in Different Pressure Vessel Steels

<i>Element</i>	<i>A302B</i> 2.2×10^{23} $n m^{-2}$	<i>A533B</i> 1×10^{23} $n m^{-2}$	<i>16MND5</i> 1.4×10^{24} $n m^{-2}$	<i>16MND5</i> 1.4×10^{24} $n m^{-2}$
Mo	56	63.6 ± 1.4	61.0 ± 2.1	63.0 ± 6.3
Fe	8	2.4 ± 0.4	—	1.9 ± 1.7
Cr	1	—	3.2 ± 0.6	—
Mn	—	2.1 ± 0.4	1.8 ± 0.5	—
C	35	31.4 ± 1.4	30.8 ± 1.9	32.7 ± 6.1
O	—	0.26 ± 0.15	—	—
N	—	0.17 ± 0.12	—	—
P	—	0.09 ± 0.09	—	1.9 ± 1.7

Data are in atomic percent.

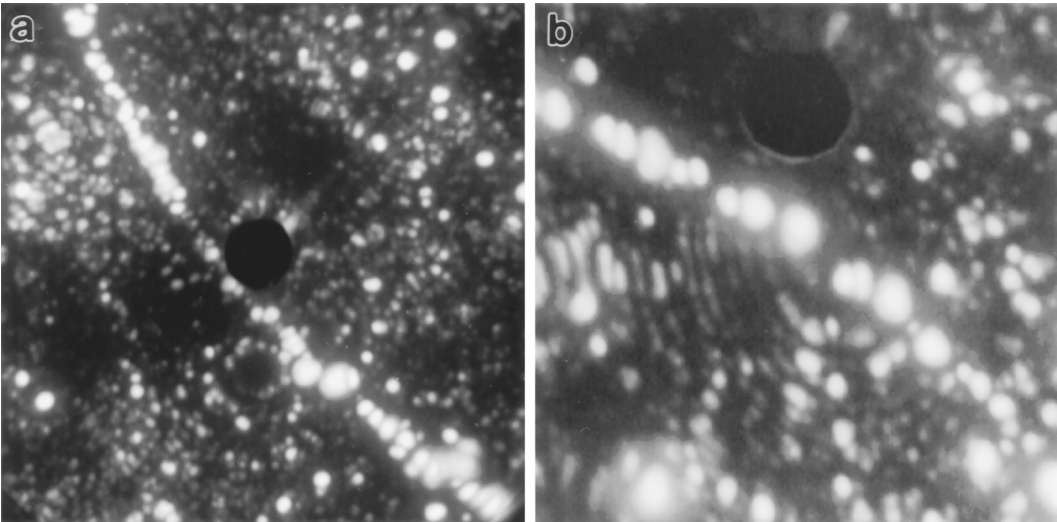


FIG. 11. Field ion micrographs of decorated boundaries in (a) an A533B submerged arc weld, and (b) a Russian VVER 440 steel.

POSTIRRADIATION ANNEALING STUDIES

If embrittlement can be reduced or eliminated, it should be possible to extend the service life of a nuclear reactor with considerable returns in economics and environmental impact. Several studies of mechanical properties have demonstrated that the embrittlement may be dramatically reduced or even eliminated by annealing the pressure vessel at a low temperature (343 to 454°C) [51–55]. The upper temperature of the annealing treatment is limited by the

magnitude of the stresses that are generated in the vessel. These low temperature postirradiation annealing treatments are designed to reduce the number of intragranular precipitates or hardening centers in the material.

Pareige et al. [32] characterized two types of materials from the B & W Master Integrated Reactor Vessel Surveillance Program. The first material was a SA-508, class 2 forging steel, with a nominal copper content of 0.02 wt. %. The second material was a typical Mn–Mo–Ni weld wire/Linde

Table 5 Summary of the Average Phosphorus Coverage at Lath and Grain Boundaries as Measured in the Atom Probe and Predicted by the McLean Model of Equilibrium Segregation

Material	Fluence ($n\ m^{-2}$) $E > 1\text{MeV}$	P Content (at. %)	Γ_i atoms cm^{-2}	Coverage, monolayers	Prediction, monolayers
A533B	Unirradiated	0.011	5.7×10^{13}	3%	5%
	1×10^{23}	0.011	1.8×10^{14}	10%	
VVER 440	Unirradiated	0.032	8.2×10^{13}	5%	7%
VVER 1000	Unirradiated	0.016	1.3×10^{14}	8%	5%
Weld 28	Unirradiated	0.045	2.0×10^{14}	11%	10%
	1×10^{23}	0.045	4.0×10^{14}	24%	
Weld 37	Unirradiated	0.058	2.8×10^{14}	13%	12%
	1×10^{24}	0.058	9.0×10^{14}	54%	

80 flux submerged arc weld, representative of the materials used to fabricate the belt-line shell course regions of the Oconee Unit-3 and Arkansas Unit-1 vessels. The copper content in the matrix of the weld material was depleted from the bulk level of 0.24at.% Cu to 0.14 ± 0.03 at.% Cu after the stress-relief heat treatment of 29 h at 593–621°C followed by a furnace cool to 310°C at a rate of $\sim 8^\circ$ C per h. The copper level in the matrix was reduced to 0.13 ± 0.04 and 0.05 ± 0.01 at.% Cu after neutron irradiation to fluences of 0.66 and 3.5×10^{23} n m⁻² ($E > 1$ MeV), respectively. Annealing the higher fluence material for 168 h at 454°C resulted in a further reduction of the matrix copper content to 0.04 ± 0.02 at.% Cu. Annealing the higher fluence material for 29 h at 610°C was found to increase the copper level in the matrix to 0.17 ± 0.04 at.% Cu.

An atom probe characterization of a 200-mm-thick section of the beltline submerged arc weld (designated a Babcock and Wilcox WF-70 weld) of the Midland Unit I pressurized water reactor was performed by Miller and Russell [33]. This weld was fabricated with the use of copper-coated welding wires and Linde 80 flux, and is known to be a low upper shelf (LUS) energy, high copper weld. This atom probe study has demonstrated that the copper in solution in the matrix of an unirradiated pressure vessel steel weld after a standard postweld heat treatment of 22.5 h at $607 \pm 14^\circ$ C was 0.119 ± 0.007 at.% Cu. This value was found to decrease to 0.088 ± 0.012 at.% Cu after annealing for 168 h at 454°C and to 0.058 ± 0.008 at.% Cu after neutron irradiation in a test reactor to a fluence of 1.1×10^{23} n m⁻² ($E > 1$ MeV) at a temperature of 288°C. An additional decrease in copper level to 0.050 ± 0.010 at.% Cu was measured by annealing the neutron irradiated material for 168 h at 454°C. These values and trends are in good agreement to previous results from a Babcock and Wilcox weld [34].

Both studies concluded that annealing neutron-irradiated pressure vessel steel welds appeared to reduce embrittlement by coarsening the copper-enriched precipi-

tates and decreasing the matrix copper content. Because the measured copper levels were significantly lower than those in the matrix after the stress-relief treatment, these results predict that the amount of reirradiation embrittlement due to copper precipitation should be significantly lower than during the initial neutron irradiation. These atom probe studies have also shown that the susceptibility of pressure vessel steels to embrittlement could be reduced by annealing the steel at an intermediate temperature of 450 to 500°C after the stress-relief treatment and prior to service.

The 16MND5 steel from the Chooz A reactor was also examined by Pareige et al. [31] after annealing for 2 and 100 h at 450°C. The size of the copper clusters was found to decrease to 1–2nm diameter after annealing for 2 h and then increase to 3–4nm diameter after annealing for 100 h. The copper level in the copper-enriched clusters was also found to increase significantly from 1% Cu after the irradiation to 30% Cu after 2 h and to 60% Cu after 100 h at 450°C. In conjunction with hardness and SANS results, it was concluded that the neutron-induced copper clusters partially dissolve in that the Si, Ni, and Mn return to the solid solution on annealing and then the remaining copper-enriched cluster acts as a nuclei for the pure copper precipitates.

LONG TERM THERMAL AGING

To study the potential effects of long term thermal aging, atom probe characterizations of the microstructure of as-fabricated and long-term thermally aged ($\sim 100,000$ h at 280°C) surveillance materials from commercial reactor pressure vessel steels have been performed by Pareige et al. [34]. This microstructural study focused on the quantification of the compositions of the matrix and carbides. The atom probe results indicate that there was no significant microstructural evolution after a long-term thermal exposure in typical Mn–Mo–Ni weld wire, Linde 80 flux submerged arc weld,

SA-533 Grade B plate, and SA-508 Class 2 forging materials.

The average copper solute concentration determined in the ferritic matrix after thermal aging was found to be consistent with the nominal level for the two plates and the forging materials. Copper depletion from 0.24at.% Cu to 0.17at.% Cu was observed in the matrices of welds of both unaged and thermally aged materials. This depletion occurred during the stress-relief heat treatment that was performed at a temperature between 593 and 621°C and subsequent furnace cool rather than the thermal aging treatment.

Molybdenum-containing carbides were frequently observed in both unaged and thermally aged specimens. The size of the observed carbides was determined to be between 5 and 20nm. The small carbides were found to have a disc, needle, or spherical shape, whereas the larger precipitates are generally spherical. The Mo:C ratio, in both the unaged and thermally aged materials, was close to that of Mo₂C. Some evidence of molybdenum atoms was found in the vicinity of dislocations and it was sometimes associated with carbon and phosphorus. The grain boundaries were decorated with a 12nm-thick layer of molybdenum carbide precipitates.

The compositions of the cementite precipitates were found to be in good agreement with Thermocalc™ predictions for materials aged at 593–620°C. This agreement indicates that long-term thermal aging has no significant impact on the evolution of the microchemistry of cementite carbides. The cementite compositions were similar to those determined from cementite precipitates in the Chooz A pressure vessel steel and weld metal.

It was concluded that the atom probe comparisons of materials under these conditions was consistent with the measured mechanical properties, such as the ductile-to-brittle transition temperature measured in Charpy V-notch impact tests, and that no significant changes in either the microstructure or the mechanical properties has been observed.

MODEL ALLOYS

Model alloys have been used in parallel with pressure vessel steels to evaluate the effect of radiation. These studies can be divided in two different categories, namely, studies of model alloys after neutron irradiation treatments representative of that in a nuclear reactor, and studies of model alloys after higher temperature isothermal aging treatments.

The first study on model alloys that is related to the embrittlement of the pressure vessel was performed by Goodman et al. in 1973 [35]. In this study, the size, number density, and compositions of the precipitates that formed in a binary Fe-1.4at.% Cu model alloy during thermal aging at 500°C were characterized by field ion microscopy and atom probe analysis. In addition, some supporting transmission electron microscopy was performed on the material after the longer aging times. The mean diameter of the particles at peak strength was determined to be 2.4nm. The mean particle size was found to follow a $t^{0.5}$ relationship with aging time, t , and a copper diffusivity of $\sim 2 \times 10^{21} \text{m}^2 \text{s}^{-1}$ was estimated. The number density of the particles when they were first visible was of the order of 10^{24}m^{-3} , and this value rapidly decreased after the peak strength of the alloy was reached. The average copper content of the initial precipitates ($\sim 47\%$ Cu after 1 h aging) was found to be significantly lower than that of the equilibrium ϵ phase, whereas, after aging for 120 h, they were consistent (93% Cu) with that of the equilibrium phase. The results of Worrall et al. [36] on similar alloys were in reasonable agreement. A composition of 95% Cu was measured in a later 3D atom probe study of one precipitate in an Fe-1.2% Cu-1.4% Ni alloy aged close to the peak hardness (2 h at 550°C) [37]. However, there is significant confusion about the true size of this precipitate (2 or 4 to 5nm), which makes comparison with the previous studies difficult [19].

In 1978, Brenner et al. [38] detected very fine darkly imaging features in a field ion microscopy study of an Fe-0.34% Cu model

alloy after neutron irradiation to a fluence of $3 \times 10^{23} \text{ n m}^{-2}$ at a temperature of 290°C . The size of these generally spherical features ranged from 0.4 to 1.6 nm, with a mean diameter of 0.6 nm, and were present at a number density of $8 \times 10^{17} \text{ cm}^{-3}$. Although no atom probe microchemical analyses were performed in this study to differentiate between microvoids and copper-enriched precipitates, Brenner et al. tentatively identified these features as copper-stabilized microvoids, and concluded that they were responsible for radiation-induced embrittlement of copper-containing ferritic steels.

A comparison between a thermally aged model Fe-1.1at.% Cu-1.4% Ni alloy and a neutron-irradiated Fe-0.22at.% Cu-0.70% Ni model steel was performed by Pareige et al. [39]. This study revealed that the composition of the copper clusters was different in the model alloy than in the pressure vessel steel. The low temperature copper solubilities have been determined in the same Fe-1.1at.% Cu-1.4% Ni alloy by Miller et al. [40] after long term isothermal aging at 300, 400, 500, 550, and 600°C . The results are summarized in Table 6. A small depletion in copper was found in the matrix after aging for 4,000 h at 300°C , and significantly larger depletions were observed at the higher temperatures. The kinetics of copper precipitation was found to have an activation energy of 250 kJ mol^{-1} . An atom map of the copper distribution in this material aged for 10,000 h at 300°C is shown in Fig. 12. Some small copper-enriched regions are evident, indicating that phase separation can occur in highly supersaturated Fe-Cu-Ni alloys at these low temperatures.

Pareige [41] has also characterized an Fe-1.4% Cu model alloy after neutron irradiation to a fluence of $5.5 \times 10^{23} \text{ n m}^{-2}$ at a temperature of 290°C , and a flux of $2.8 \times 10^{17} \text{ n m}^{-2} \text{ s}^{-1}$. A copper atom map showing a high density ($2 \times 10^{24} \text{ m}^{-3}$) of 2 to 4 nm diameter copper precipitates obtained from this material in the tomographic atom probe [41] is shown in Fig. 13(a). In this type of representation, each dot indicates the location of an individual copper atom, and the copper precipitates are evident

Table 6 Change in Copper Content of the Matrix of an Fe-1.1% Cu, 1.4% Ni Model Alloy as a Function of Aging Time and Temperature

Time (h)	Copper concentration, at. %		
	300°C	400°C	500°C
0.5	—	—	0.47 ± 0.11
1	—	0.92 ± 0.08	0.31 ± 0.10
4	—	—	0.13 ± 0.03
10	—	0.91 ± 0.09	0.13 ± 0.03
100	—	0.54 ± 0.08	0.073 ± 0.02
168	0.93 ± 0.06	—	—
1,000	0.82 ± 0.06	0.12 ± 0.03	0.082 ± 0.03
4,000	0.80 ± 0.05	0.085 ± 0.01	—
	550°C	600°C	850°C AQ
5	—	—	0.91 ± 0.04
1,000	0.12 ± 0.03	0.18 ± 0.03	—

from the local high density of spots. A composition profile through one of the copper precipitates and the distribution of the maximum copper concentrations measured in these precipitates are shown in Fig. 13(b) and (c), respectively. It is evident from these data that there is a significant distribution in the copper level from one precipitate to another in this neutron-irradiated material, and that the copper level is significantly lower (0.04% Cu) than that predicted from materials thermally aged at higher temperatures. Pareige also studied the same material after electron irradiation at the same temperature to a fluence of $9 \times 10^{23} \text{ e m}^{-2}$ with a flux of $4 \times 10^{17} \text{ e m}^{-2} \text{ s}^{-1}$, and found 2 nm-diameter precipitates containing 95% Cu at a number density of 10^{24} m^{-3} . This indicates that, even if the NRT displacements per atom are not the same (5.4×10^{-5} and 7.5×10^{-2} for electron and neutron, respectively), the phase transformation under these irradiation conditions does not follow the same path.

Some model pressure vessel steels were also characterized by Miller et al. [42, 43] in 1987. In this systematic study, five model alloys were produced from a split melt with a base composition representative of a



FIG. 12. Copper atom map in an Fe-1.1%Cu-1.4% Ni alloy aged for 10,000 h at 300°C. Small copper-enriched regions are evident. Box is $13 \times 13 \times 101$ nm. Individual random copper atoms have been omitted for clarity.

low manganese (0.01at.% Mn) pressure vessel steel and with low and high levels of copper (<0.008 and 0.22at.% Cu), nickel (0.011 and -0.67% Ni), and phosphorus (-0.007 and 0.041at.% P). These materials were examined after neutron irradiation for 1600 h to a fluence of $4.6 \times 10^{23} \text{ n m}^{-2}$ ($E > 1\text{MeV}$) at a temperature of 288°C. The matrix copper level was found to be significantly depleted in the 0.22at.% Cu steels after neutron irradiation (0.03at.% Cu in the FeCu, 0.07% Cu in the Fe-Cu-Ni and 0.08% Cu in the Fe-Cu-Ni-P alloy) compared to the 0.19 at. % Cu measured in a Fe-Cu alloy annealed for 1600 h at 288°C. No clusters or precipitates were observed in the thermally aged alloy. A high number density of ultrafine ($\sim 2\text{nm}$) darkly imaging copper-enriched clusters were observed in all neutron-irradiated copper-containing steels. In the Fe-Cu-Ni alloy, the clusters contained approximately 50% Cu, and were also enriched in nickel. Similar results were observed in an irradiated Fe-0.31at.% Cu-0.51% Ni-0.46% C alloy. The maximum phosphorus-to-copper ratio in the phosphorus-free Fe-Cu and Fe-Cu-Ni alloys was -2%. However, in the Fe-Cu-Ni-P alloy, phosphorus-to-copper ratio of the clusters was found to be between 25 and 50% in $\sim 30\%$ of the cases, indicating a copper-phosphide cluster or precipitate. The nickel level was also found to be higher in the vicinity of these clusters. In the copper-free Fe-Ni-P and Fe-Ni alloys, several ultrafine spherical phosphorus-rich clusters were detected. The number density of the clusters in the phosphorus-containing alloy was significantly larger due to the higher

phosphorus content of the alloy. Both nickel and carbon were found to be associated with these phosphorus clusters.

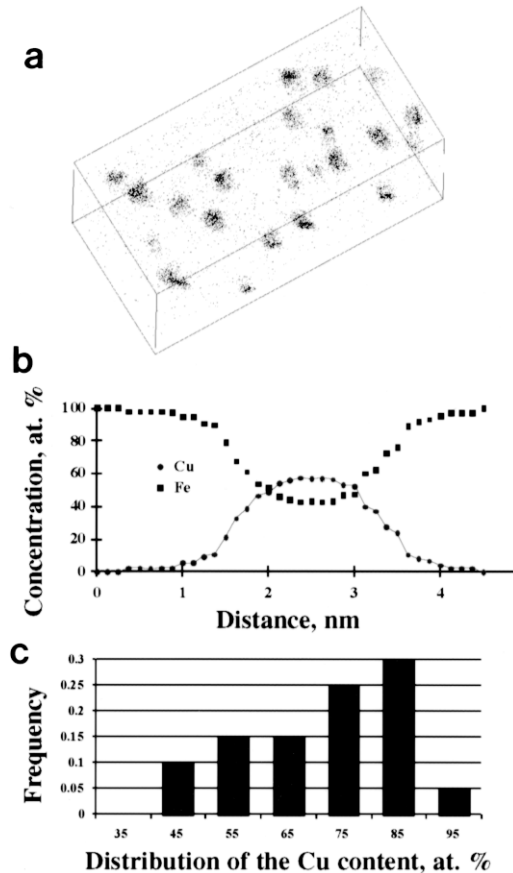


FIG. 13. (a) Copper atom map ($15 \times 15 \times 30$ nm), (b) composition profile through a 2.5nm-diameter copper precipitate, and (c) the distribution of the copper content of the copper precipitates from a neutron-irradiated Fe-1.4% Cu alloy ($T = 290^\circ\text{C}$, dose = $5.5 \times 10^{23} \text{ n m}^{-2}$, flux = $2.8 \times 10^{17} \text{ n m}^{-2} \text{ s}^{-1}$).

SUMMARY

Atom probe studies have provided the first direct evidence of copper-enriched clusters and phosphorus clusters in the matrix of neutron-irradiated pressure vessel steels. The copper-enriched clusters were also found to be enriched in other solutes particularly nickel, manganese, phosphorus, and silicon. In addition, several types of intragranular and intergranular precipitates have been characterized in these materials. Atom probe studies have also revealed a complex pattern of segregation of various solutes including phosphorus, nickel, and manganese to grain and lath boundaries in some pressure vessel steels. Furthermore, atom probe analysis has provided the only true quantitative measurement of the matrix solute content so that the true copper content of the matrix prior to irradiation and after irradiation can be determined. These data have demonstrated the importance of the stress-relief temperature for weldments in reducing the amount of copper available for cluster/precipitate formation in high-copper steels. Also, the atom probe has been able to provide unique microchemical data that have been very important in the interpretation of results obtained from other analytical techniques such as small angle neutron scattering (SANS).

The information obtained by the atom probe technique has provided experimental evidence that has led to a basic understanding of the causes of embrittlement of these pressure vessels and the mechanisms that operate during postirradiation annealing treatments.

The authors wish to thank S. P. Grant for his continued interest and encouragement of atom probe studies of RPV materials. This research was sponsored by the Division of Materials Sciences, U.S. Department of Energy, under contract DE-AC05-96OR22464 with Lockheed Martin Energy Research Corp., by the Office of Nuclear Regulatory Research, U.S. Nuclear Regulatory Commission under inter-agency agreement DOE 1886-N695-3W with the U.S.

Department of Energy, and through the SHaRE Program under contract DE-AC05-76OR00033 with Oak Ridge Associated Universities. This research was conducted utilizing the Shared Research Equipment User Program facilities at ORNL. Studies of the French pressure vessel steels and some model alloys were performed at the "Equipe de Sonde Atomique et Microstructures" of the GMP-UMR CNRS 6634 of the Rouen University and were financially supported by Electricité de France Département Etude des Matériaux" under EDF/CNRS contracts.

References

1. E. W. Muller, J. A. Panitz, and S. B. McLane: The atom-probe field ion microscope. *Rev. Sci. Instrum.* 39:83-86 (1968).
2. M. K. Miller, A. Cerezo, M. G. Hetherington, and G. D. W. Smith: *Atom Probe Field Ion Microscopy*, Oxford University Press, Oxford, UK (1996).
3. G. R. Odette and G. E. Lucas: Irradiation embrittlement of reactor pressure vessel steels: Mechanisms, models and data correlations. In *Radiation Embrittlement of Nuclear Reactor Pressure Vessel Steels; An International Review (second volume) ASTM STP 909*, L. E. Steele, ed., American Society for Testing and Materials, Philadelphia, PA pp. 206-241 (1986).
4. *Radiation Embrittlement of Nuclear Reactor Pressure Vessel Steels, An International Review, ASTM STP 1170*, L. E. Steele, ed., American Society for Testing and Materials, Philadelphia, PA (1993).
5. N. N. Alekseenko, A. Amaev, I. Gorynin, and V. A. Nikolaev: *Radiation Damage of Nuclear Power Plant Pressure Vessel Steels*, American Nuclear Society, La Grange Park, IL (1997).
6. J. R. Hawthorne: *Exploratory Studies of Element Interactions and Composition Dependencies in Radiation Sensitivity Development*, USNRC Report NUREG/CR-4437 (MEA-2113) (November 1985).
7. G. R. Odette, C. L. Liu, and B. D. Wirth: On the composition and structure of nanoprecipitates in irradiated pressure vessel steels. In *Microstructure Evolution During Irradiation, Symposium Proceedings, Vol. 439*, I. M. Robertson, G. S. Was, L. W. Hobbs, and T. D. de la Rubia, eds., Materials Research Society, Pittsburgh, PA, pp. 457-469 (1997).
8. G. R. Odette: Radiation-induced microstructural evolution in reactor pressure vessel steels. In *Microstructure of Irradiated Materials, Symposium Proceedings, Vol. 373*, I. M. Robertson, L. E. Rehn, S. J.

- Zinkle, and W. J. Phythian, eds., Materials Research Society, Pittsburgh, PA, pp. 137–148 (1995).
9. M. K. Miller, M. G. Hetherington, and M. G. Burke: Atom probe field-ion microscopy: A technique for microstructural characterization of irradiated materials on the atomic scale. *Metall. Trans.* 20A: 2651–2661 (1989).
 10. M. K. Miller and S. S. Brenner: *An Atom Probe Study of Irradiated Pressure Vessel Steel*. Proc. 28th Int. Field Emission Symposium, 27–31 July 1981, L. W. Swanson and A. Bell, eds., The Oregon Graduate Center, Beaverton, OR, pp. 242–244 (1981).
 11. M. K. Miller and S. S. Brenner: FIM/atom probe study of irradiated pressure vessel steels. *Res. Mechan.* 10:161–168 (1984).
 12. M. K. Miller, J. A. Spitznagel, S. S. Brenner, and M. G. Burke: *Microanalytical Investigation of Light Water Reactor Materials Using the Atom Probe*. Proc. 2nd Int. Symp. on Environmental Degradation of Materials in Nuclear Power Systems—Water reactors, J. T. A. Roberts, J. R. Weeks, and G. J. Theus, eds., American Nuclear Society, La Grange Park, IL, pp. 523–528 (1986).
 13. S. P. Grant, S. L. Earp, S. S. Brenner, and M. G. Burke: *Phenomenological Modeling of Radiation Embrittlement in Light Water Reactor Vessels with Atom Probe and Statistical Analysis*. Proc. 2nd Int. Symp. on Environmental Degradation of Materials in Nuclear Power Systems—Water Reactors, J. T. A. Roberts, J. R. Weeks, and G. J. Theus, eds., American Nuclear Society, La Grange Park, IL, pp. 385–392 (1986).
 14. M. G. Burke and S. S. Brenner: A microstructural investigation of irradiated pressure vessel steel weld metal. *J. Phys.* 47-C2:239–244 (1986).
 15. M. K. Miller and M. G. Burke: Characterization of irradiated A533B pressure vessel steel weld. *J. Phys.* 48-C6:429–434 (1987).
 16. M. K. Miller and M. G. Burke: *Microstructural characterization of PWR Steel Using the Atom Probe Field-Ion Microscope*. Proc. 3rd Int. Symp. on Environmental Degradation of Materials in Nuclear Power Systems—Water Reactors, G. J. Theus and J. R. Weeks, eds., The Metallurgical Society, Pittsburgh, PA, pp. 141–149 (1988).
 17. M. G. Burke and M. K. Miller: Solute clustering and precipitation in pressure vessel steels under low fluence irradiation conditions. *J. Phys.* 49-C6: 283–288 (1988).
 18. M. K. Miller and M. G. Burke: *Fine Scale Microstructural Characterization of Pressure Vessel Steels and Related Materials Using APFIM* Proc. 14th Int. Symp. On Effects of Radiation on Materials ASTM-STP 1046, vol. 2, N. H. Packan, R. E. Stoller, and A. S. Kumar, eds., American Society for Testing and Materials, Philadelphia, PA, pp. 107–126 (1990).
 19. M. K. Miller and M. G. Burke: An atom probe field ion microscopy study of neutron-irradiated pressure vessel steels. *J. Nucl. Mater.* 195:68–82 (1992).
 20. P. Pareige, J. C. Van Duysen, and P. Auger: An APFIM study of the microstructure of a ferrite alloy after high fluence neutron irradiation. *Appl. Surf. Sci.* 67:342–347 (1993).
 21. P. Auger, P. Pareige, M. Akamatsu, and J.-C. Van Duysen: Microstructural characterization of atom clusters in irradiated pressure vessel steels and model alloys. *J. Nucl. Mater.* 211:194–201 (1994).
 22. M. Akamatsu, J. C. Van Duysen, P. Pareige, and P. Auger: Experimental evidence of several contributions to the radiation damage in ferritic alloys. *J. Nucl. Mater.* 225:192–195 (1995).
 23. P. Auger, P. Pareige, M. Akamatsu, and D. Blavette: APFIM investigation of clustering in neutron-irradiated Fe-Cu alloys and pressure vessel steels. *J. Nucl. Mater.* 225:225–230 (1995).
 24. M. K. Miller and M. G. Burke: *An APFIM Survey of Grain Boundary Segregation and Precipitation in Irradiated Pressure Vessel Steels*, Proc. 16th Int. symp. on Effects of Radiation in Materials-ASTM STP 1175, A. S. Kumar, D. S. Gelles, R. K. Nanstad, and E. A. Little, eds., American Society for Testing and Materials, Philadelphia, PA, pp. 492–502 (1993).
 25. M. K. Miller, R. Jayaram, P. J. Othen, and G. Brauer: *Atom Probe Field Ion Microscopy Characterizations of VVER Steels*. Proc. 6th Int. Symp. on Environmental Degradation of Materials in Nuclear Power Systems—Water Reactors, R. E. Gold and E. P. Simonen, eds., The Minerals, Metals and Materials Society, Warrendale, PA, pp.161–169 (1993).
 26. M. K. Miller, R. Jayaram, P. J. Othen, and G. Brauer: APFIM characterization of 15Kh2MFA Cr-Mo-V and 15kh2NMFA Ni-Cr-Mo-V type steels. *Appl. Surface Sci.* 76/77:242–247 (1994).
 27. M. K. Miller, R. Jayaram, and K. F. Russell: Characterization of phosphorus segregation in neutron-irradiated Russian pressure vessel steel weld. *J. Nucl. Mater.* 225:215–224 (1995).
 28. M. K. Miller, R. Jayaram, and K. F. Russell: *Characterization of Phosphorus Segregation in Neutron-Irradiated Pressure Vessel Steels by Atom Probe Field-Ion Microscopy*. Proc. Microstructure of Irradiated Materials, Vol. 373, I. M. Robertson, L. E. Rehn, S. J. Zinkle, and W. J. Phythian, eds., Materials Research Society, Pittsburgh, PA, pp. 113–118 (1995).
 29. M. K. Miller and K. F. Russell: APFIM characterization of a high phosphorus Russian RPV weld. *Appl. Surface Sci.* 94/95:378–383 (1996).
 30. P. Pareige, P. Auger, S. Miloudi, J. C. Van Duysen, and M. Akamatsu: Microstructural evolution of the CHOOZ A PWR surveillance program material: Small angle neutron scattering and tomographic atom probe studies. *Ann. Phys. C2* 22:117–124 (1997).8
 31. P. Pareige, P. Auger, S. Welzel, J. C. Van Duysen,

- and S. Miloudi: *Annealing of a Low Copper Steel: Hardness, SANS, Atom Probe and Thermoelectric Power Investigations*. Proc. 19th Int. Symp. Effects of Radiation on Materials, ASTM STP 1366, M. L. Hamilton, A. S. Kumar, S. T. Rosinski, and M. L. Grossbeck, eds., American Society for Testing and Materials, Philadelphia, PA (in press).
32. P. Pareige, K. F. Russell, R. E. Stoller, and M. K. Miller: Influence of long-term thermal aging on the microstructural evolution of nuclear reactor pressure vessel materials: An atom probe study. *J. Nucl. Mater.* 250:176–183 (1997).
 33. M. K. Miller and K. F. Russell: Atom probe characterization of copper solubility in the Midland weld after neutron irradiation and thermal annealing. *J. Nucl. Mater.* 250:223–228 (1997).
 34. P. Pareige, R. E. Stoller, K. F. Russell, and M. K. Miller: Atom probe characterization of the microstructure of nuclear pressure surveillance materials after neutron irradiation and after annealing treatments. *J. Nucl. Mater.* 249:165–174 (1997).
 35. S. R. Goodman, S. S. Brenner, and J. R. Low: An FIM-atom probe study of the precipitation of copper from iron 1.4 At. Pct copper: Part I field ion microscopy, and part II, atom probe analysis. *Metal. Trans.* 4:2363–2378 (1973).
 36. G. M. Worrall, J. T. Buswell, C. A. English, M. G. Hetherington, and G. D. W. Smith: A study of the precipitation of copper particles in a ferrite matrix. *J. Nucl. Mater.* 148:107–114 (1987).
 37. J. T. Buswell, C. A. English, M. G. Hetherington, W. J. Phythian, G. D. W. Smith, and G. M. Worrall: *An Analysis of Small Clusters Formed in Thermally aged and Irradiated FeCu and FeCuNi Model Alloys*. Proc. 14th Int. Symp. On Effects of Radiation on Materials ASTM-STP 1046, vol. 2, N. H. Packan, R. E. Stoller, and A. S. Kumar, eds., American Society for Testing and Materials, Philadelphia, PA, pp. 127–153 (1990).
 38. S. S. Brenner, R. Wagner, and J. A. Spitznagel: Field-ion microscope detection of ultra-fine defects in neutron-irradiated Fe-0.34 Pct Cu alloy. *Metal. Trans.* 9A:1761–1764 (1978).
 39. P. J. Pareige, K. F. Russell, and M. K. Miller: APFIM studies of the phase transformation in thermally aged ferritic FeCuNi alloys: Comparison with aging under neutron irradiation. *Appl. Surface Sci.* 94/95: 363–369 (1996).
 40. M. K. Miller, K. F. Russell, P. Pareige, M. J. Starink, and R. C. Thomson: Low temperature copper solubilities in Fe-Cu-Ni. *Mater. Sci. Eng.* A250: 49–54 (1998).
 41. P. Pareige, P. Auger, P. Bas, and D. Blavette: Direct observation of copper precipitation in neutron-irradiated FeCu alloys by 3D atomic tomography. *Scripta Metall. Mater.* 33: 1033–1036 (1995).
 42. M. K. Miller, D. T. Hoelzer, F. Ebrahimi, J. R. Hawthorne, and M. G. Burke: Characterization of irradiated model pressure vessel steels. *J. Phys.* 48-C6: 423–428 (1987).
 43. M. K. Miller, D. T. Hoelzer, F. Ebrahimi, J. R. Hawthorne, and M. G. Burke: *Microstructural Characterization of Irradiated Fe-Cu-Ni-P Model Steels*. Proc. 3rd Int. Symp. on Environmental Degradation of Materials in Nuclear Power Systems—Water Reactors, G. J. Theus and J. R. Weeks, eds., The Metallurgical Society, Pittsburgh, PA, pp 133–139 (1988).
 44. M. K. Miller, R. E. Stoller, and K. F. Russell: Effect of neutron-irradiation on the spinodal decomposition of Fe-43% Cr model alloy, *J. Nucl. Mater.* 230: 219–225 (1996).
 45. J. T. Buswell, C. A. English, M. G. Hetherington, W. J. Phythian, G. D. W. Smith and G. M. Worrall: *Analysis of Small Clusters formed in Irradiated and Thermally Aged Copper-Containing Model Alloys*, Proc. 14th Int. Symp. on Effects of Radiation on Materials: ASTM STP 1046, N. H. Packan, R. E. Stoller and A. S. Kumar, eds., American Society for Testing and Materials, Philadelphia, PA, p.127 (1990).
 46. P. J. Othen, M. L. Jenkins, G. D. W. Smith, and W. J. Phythian: Transmission electron microscope investigations of the structure of copper precipitates in thermally-aged Fe-Cu and Fe-Cu-Ni. *Philos. Mag. Lett.* 64:383–391 (1991).
 47. M. K. Miller and G. D. W. Smith: Atom probe analysis of interfacial segregation. *App. Surface Sci.* 87/88:243–250 (1995).
 48. A. Vatter, C. A. Hipplesley, and S. G. Druce: Review of thermal aging data and its application to operating reactor pressure vessels. *Int J. Pressure Ves. Piping*, 54:31–48 (1993).
 49. S. G. Druce, G. Gage, and G. Jordan: Effect of aging on properties of pressure vessel steels. *Acta Metall.* 34:641–652 (1986).
 50. D. McLean: *Grain Boundaries in Metals*, Oxford University Press, London, p. 116 (1957).
 51. J. R. Hawthorne, H. E. Watson, and F. L. Loss: Exploratory investigations of cyclic irradiation and annealing effects on Notch Ductility of A533B weld deposits. In *Effects of Radiation on Structural Materials*, ASTM STP 683, J. A. Sprague and D. Kramer, eds., American Society for Testing and Materials, Philadelphia, PA, pp. 278–294 (1978).
 52. J. R. Hawthorne, H. E. Watson, and F. L. Loss: *Experimental Investigation of Multicycle Irradiation and Annealing Effects on Notch Ductility of A533-B Weld Deposits*. Proc. 10th Conf. on Effects of Radiation in Materials, ASTM STP 725, D. Kramer, H. R. Prager, and J. S. Perrin, eds., American Society for Testing and Materials, Philadelphia, PA, pp. 63–75 (1981).
 53. R. G. Lott, T. R. Mager, R. P. Shogan, and S. E. Yanichko: Annealing and reirradiation response of irradiated pressure vessel steels. In *Radiation Embrittlement of Nuclear Reactor Pressure Vessel Steels*, An

- International Review*, vol. 2, ASTM STP 909, L. E. Steele, ed., American Society for Testing and Materials, Philadelphia, PA, pp. 242–259 (1986).
54. J. R. Hawthorne: *Steel Impurity Element Effects on Post irradiation Properties Recovery by Annealing*. 13th Int. Symp. Influence of Radiation on Materials Properties Part II, ASTM STP 956, F. A. Garner, C. H. Hanager, and N. Igata, eds. American Society for Testing and Materials, Philadelphia, PA, pp. 461–479 (1987).
55. J. R. Hawthorne and A. L. Hiser: *Investigation of Irradiation-anneal-reirradiation (IAR) Property Trends of RPV Welds*. Proc. 5th Int. Symp. on Environmental Degradation of Materials in Nuclear Power Systems—Water Reactors, D. Cubicciotti, E. P. Simonen, and R. E. Gold, eds., American Nuclear Society, La Grange Park, IL, pp. 671–678 (1992).

Received December 1998; accepted February 1999.